Supplementary Material

# An Anionic Calcium Metal-Organic Framework Encapsulated Tb^{III} Ions as a Recyclable Luminescent Sensor for Cr^{III} and Fe^{III} ions

Min Chen[A,C] *and Wen-Ming Xu*[B]

[A] Hubei University of Education, Hubei Key Laboratory of Purification and Application of Plant Anti-Cancer Active Ingredients, Wuhan, Hubei 430205, China.

[B] Zhengzhou University of Light Industry, Henan Provincial Key Laboratory of Surface & Interface Science, Zhengzhou, Henan 450002, China.

[C] Corresponding author. Email: chem_chenmin@163.com
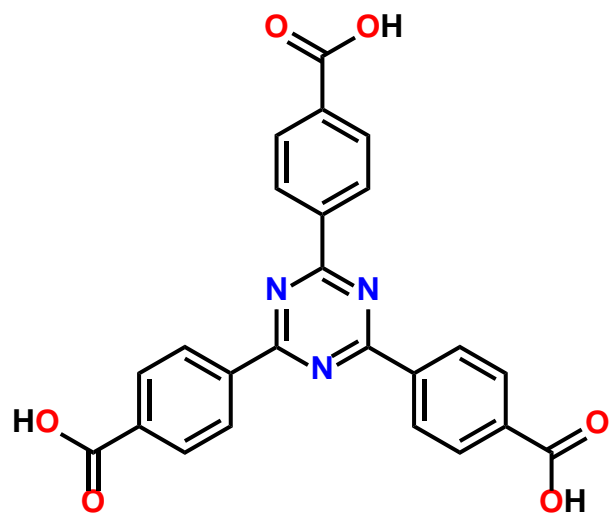
Scheme S1 Schematic drawing of the ligand H$_3$TATB.

Table S1 A comparison of the selected bond lengths [Å] and angles [°] for Ca-MOF.[a]

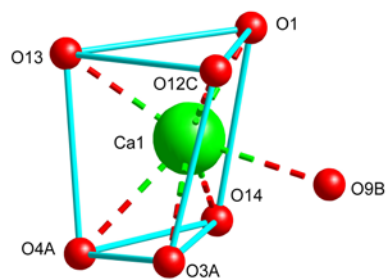| Ca-MOF			
Ca1–O14	2.269(4)	Ca1–O1	2.280(3)
Ca1–O13	2.339(3)	Ca1 O9[#2]	2.443(2)
Ca2–O3	2.304(2)	Ca3–O6	2.292(2)
Ca3–O7	2.299(2)	Ca3–O10[#6]	2.324(2)
Ca1–O12[#3]	2.361(2)	Ca2–O8[#3]	2.365(2)
Ca2–O5[#3]	2.449(2)	Ca1–O4[#1]	2.472(3)
Ca2–O11[#5]	2.483(2)	Ca2–O10[#4]	2.514(2)
Ca2–O12[#5]	2.553(2)	Ca1–O3[#1]	2.618(3)
Ca2–O6[#3]	2.667(2)	Ca2–O9[#4]	2.713(2)
Ca2–O7[#3]	3.004(3)		
O1–Ca1–O12[#3]	91.72(10)	O1–Ca1–O9[#2]	90.30(9)
O1–Ca1–O13	85.67(12)	O1–Ca1–O3[#1]	159.94(9)
O1–Ca1–O4[#1]	149.08(11)	O12[#3]–Ca1–O3[#1]	75.76(7)
O12[#3]–Ca1–O9[#2]	71.45(7)	O12[#3]–Ca1–O4[#1]	114.15(11)
O13–Ca1–O12[#3]	84.30(10)	O13–Ca1–O4[1]	80.67(12)
O13–Ca1–O3[#1]	108.15(11)	O14–Ca1–O3[#1]	99.18(16)
O14–Ca1–O1	86.18(18)	O14–Ca1–O9[#2]	85.61(16)
O14–Ca1–O4[#1]	76.34(18)	O14–Ca1–O12[#3]	156.96(16)
O14–Ca1–O13	118.33(18)	O4[#1]–Ca1–O3[#1]	50.31(9)
O9[#2]–Ca1–O3[#1]	71.01(7)	O9[#2]–Ca1–O4[#1]	113.15(9)
O13–Ca1–O9[#2]	155.29(10)	O3–Ca2–O8[#3]	93.68(11)
O3–Ca2–O11[#5]	95.13(10)	O5[#3]–Ca2–O10[#4]	91.24(9)
O3–Ca2–O7[#3]	92.00(8)	O5[#3]–Ca2–O9[#4]	84.70(8)
O3–Ca2–O10[#4]	85.74(8)	O5[#3]–Ca2–O11[#5]	80.23(10)
O8[#3]–Ca2–O11[#5]	83.71(9)	O3–Ca2–O12[#5]	78.05(7)
O8[#3]–Ca2–O6[#3]	80.11(9)	O3–Ca2–O9[#4]	71.31(9)
O5[#3]Ca2–O12[#5]	76.55(7)	O10[#4]–Ca2–O7[#3]	65.65(6)

O10$^{\#4}$–Ca2–O6$^{\#3}$	70.48(6)	O6$^{\#3}$–Ca2–O7$^{\#3}$	62.83(6)
O12$^{\#5}$–Ca2–O9$^{\#4}$	64.31(6)	O5$^{\#3}$–Ca2–O6$^{\#3}$	50.37(6)
O11$^{\#5}$–Ca2–O12$^{\#5}$	51.62(7)	O8$^{\#3}$–Ca2–O7$^{\#3}$	46.49(8)
O10$^{\#4}$–Ca2–O9$^{\#4}$	49.39(6)	O11$^{\#5}$–Ca2–O10$^{\#4}$	164.10(7)
O12$^{\#5}$–Ca2–O7$^{\#3}$	170.04(7)	O3–Ca2–O5$^{\#3}$	150.76(9)
O8$^{\#3}$–Ca2–O9$^{\#4}$	155.61(10)	O8$^{\#3}$–Ca2–O12$^{\#5}$	132.78(8)
O3–Ca2–O6$^{\#3}$	150.55(7)	O12$^{\#5}$–Ca2–O6$^{\#3}$	126.84(6)
O11$^{\#5}$–Ca2–O7$^{\#3}$	130.07(7)	O8$^{\#3}$–Ca2–O5$^{\#3}$	114.24(11)
O11$^{\#5}$–Ca2–O9$^{\#4}$	115.92(7)	O5$^{\#3}$–Ca2–O7$^{\#3}$	113.19(7)
O10$^{\#4}$–Ca2–O12$^{\#5}$	113.46(6)	O8$^{\#3}$–Ca2–O10$^{\#4}$	112.11(8)
O11$^{\#5}$–Ca2–O6$^{\#3}$	112.54(9)	O9$^{\#4}$–Ca2–O7$^{\#3}$	113.17(6)
O6$^{\#3}$–Ca2–O9$^{\#4}$	103.32(7)	O6–Ca3–O7	80.63(9)
O6–Ca3–O10$^{\#8}$	80.82(7)	O7$^{\#7}$–Ca3–O10$^{\#8}$	98.44(8)

[a] Symmetry codes: #1 = x – 1, y – 1, z; #2 = x – 1, y, z – 1; #3 = x, y, z – 1; #4 = x, y + 1, z – 1; #5 = x + 1, y + 1, z – 1; #6 = –x + 1, –y + 1, –z + 2; #7 = –x + 1, –y + 2, –z + 2; #8 = x, y + 1, z

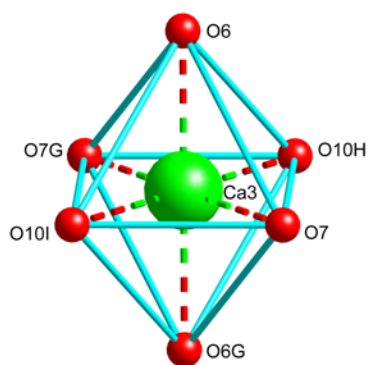**Table S2** Hydrogen bond lengths [Å] and angles [°] for Ca-MOF.

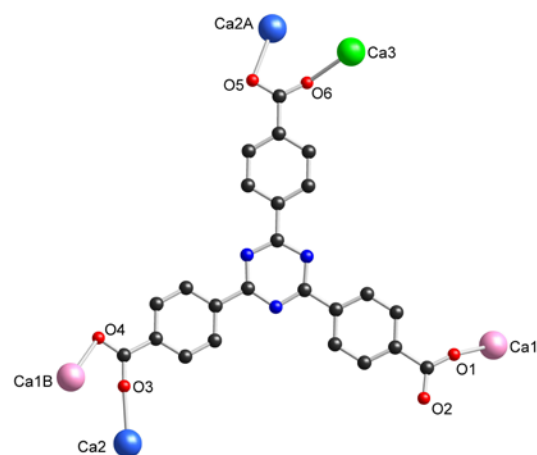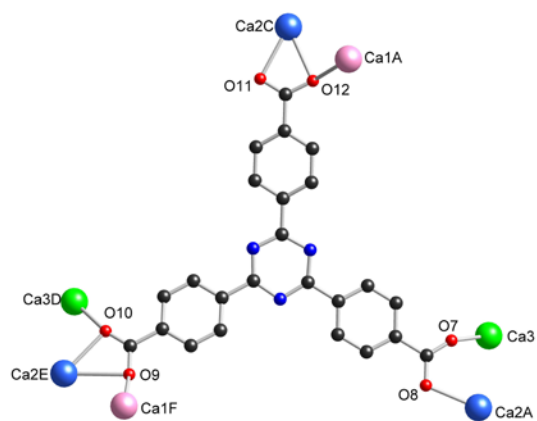| D–H···A	d(H···A) (Å)	d(D···A) (Å)	∠D–H···A (°)	Symmetry codes
N9–H9A···O5	2.41	3.03	127	x, y – 1, z
N9–H9A···O9	2.55	3.18	129	
N9–H9A···O12	2.29	3.01	139	x + 1, y, z
N9–H9B···O2	1.79	2.65	162	x + 1, y, z + 1

(a)
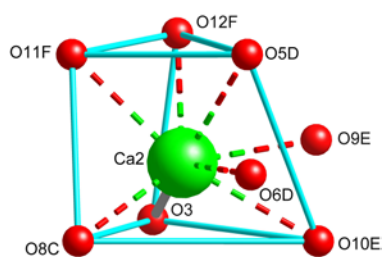
(b)

(c)

Fig. S1 The coordination polyhedron of Ca^{II} ions in Ca-MOF. Symmetry codes: $x - 1$, $y - 1$, z for A; $x - 1$, y, $z - 1$ for B; x, y, $z - 1$ for C; x, y, $z - 1$ for D; x, $y + 1$, $z - 1$ for E; $x + 1$, $y + 1$, $z - 1$ for F; $-x + 1$, $-y + 2$, $-z + 2$ for G; $-x + 1$, $-y + 1$, $-z + 2$ for H; x, $y + 1$, z for I.
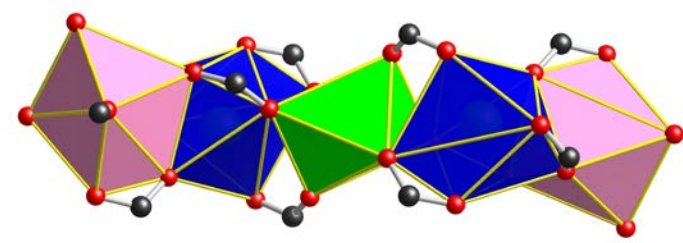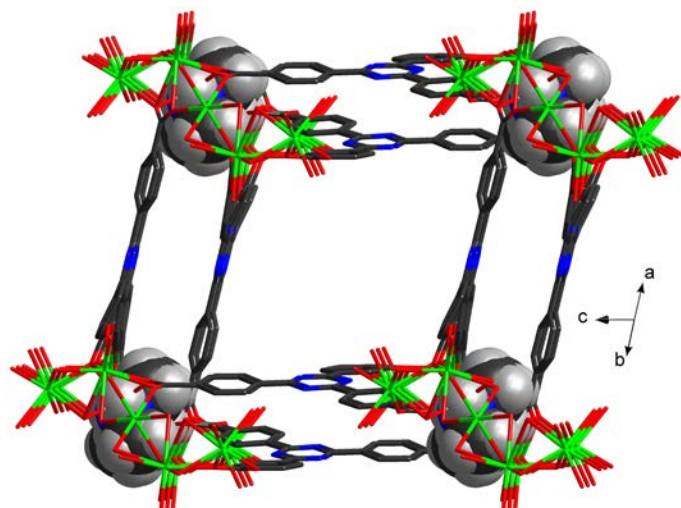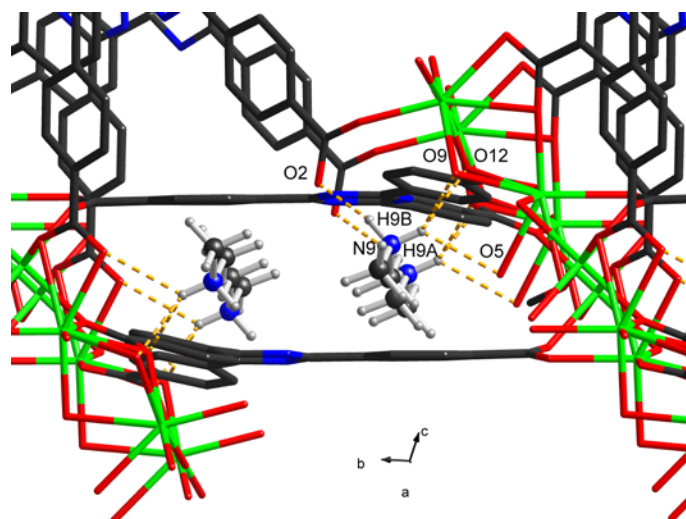
(a)

(b)

Fig. S2 View of the coordination modes of TATB ligands. Symmetry codes: $A = x, y, z + 1$; $B = x + 1, y + 1, z$; $C = x - 1, y - 1, z + 1$; $D = x, y - 1, z$; $E = x, y - 1, z + 1$; $F = x + 1, y, z + 1$.

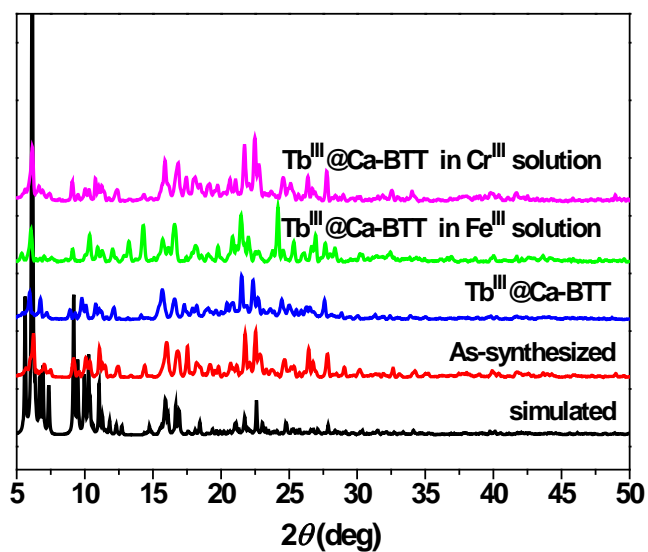**Fig. S3** View of the pentanuclear SBU. The Ca1, Ca2, Ca3 ions are shown in pink, blue, and green, respectively.
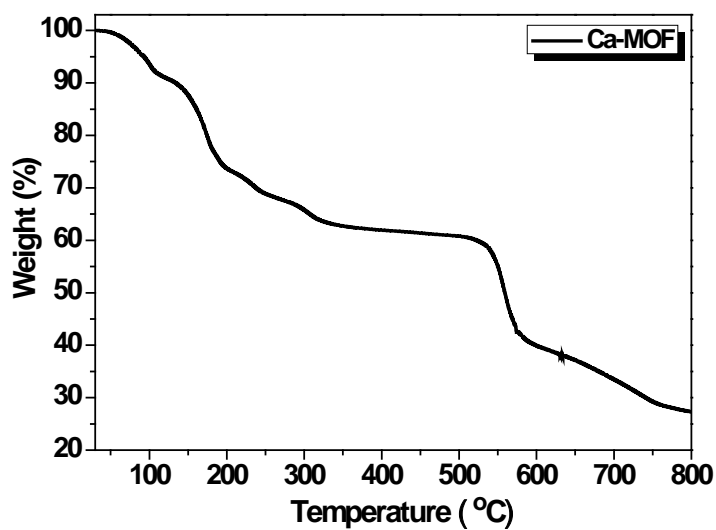
(a)

(b)

Fig. S4 (a) View of the location of $[(CH_3)_2NH_2]^I$ cations in the 3-D framework. (b) View of the hydrogen-bonding interactions (orange dashed lines) between $[(CH_3)_2NH_2]^I$ cations and carboxylate groups.
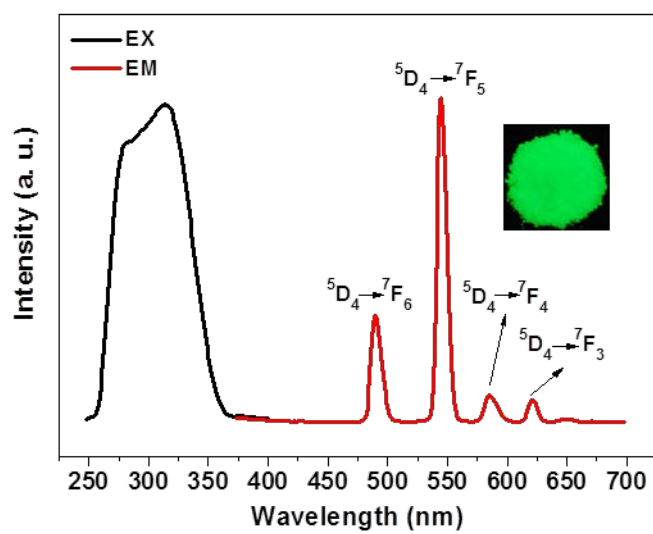
Fig. S5 Power X-ray diffraction patterns of Ca-MOF and Tb^{III}@Ca-MOF after five recyclable experiments.
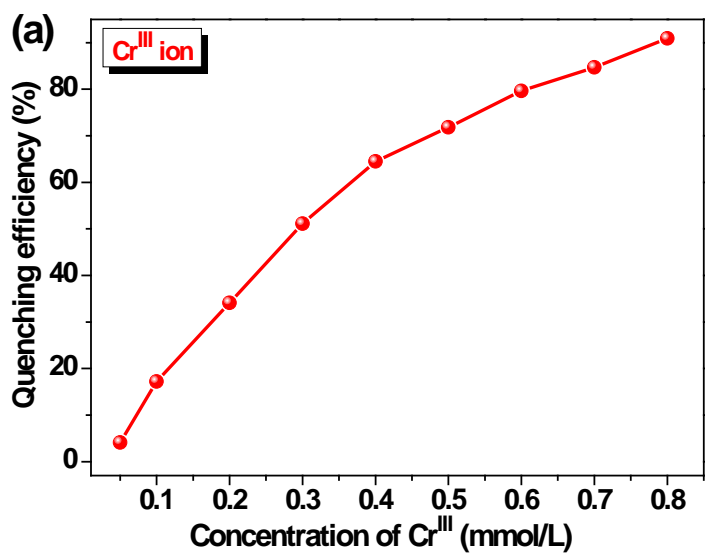

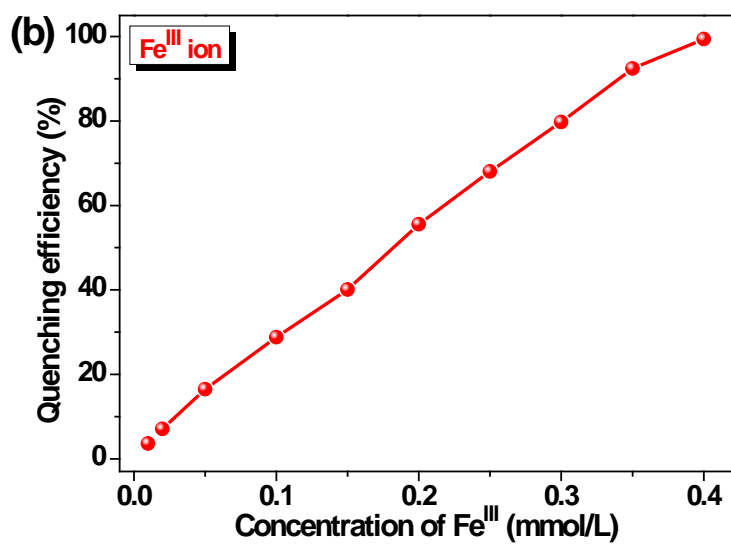
Fig. S6 TG curve of Ca-MOF.

Fig. S7 Excitation (black line) and emission (red line) spectra of Tb^{III}@Ca-MOF. The inset is the corresponding luminescence picture under UV-light irradiation of 254 nm.
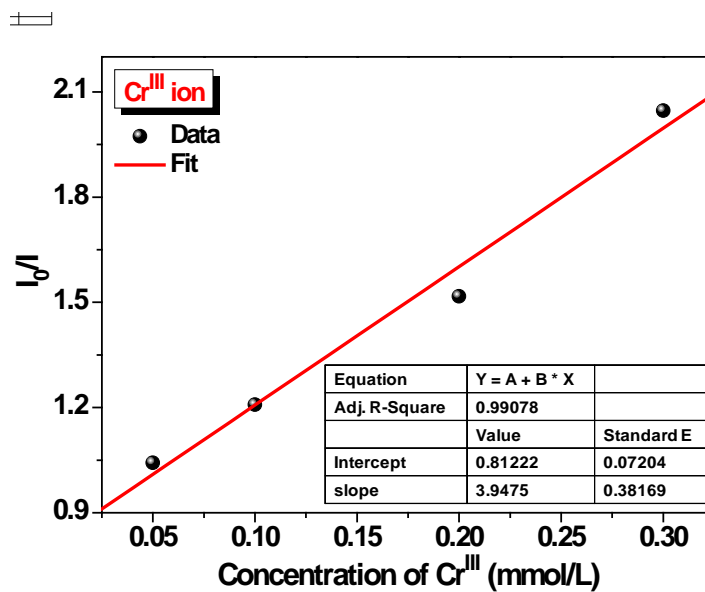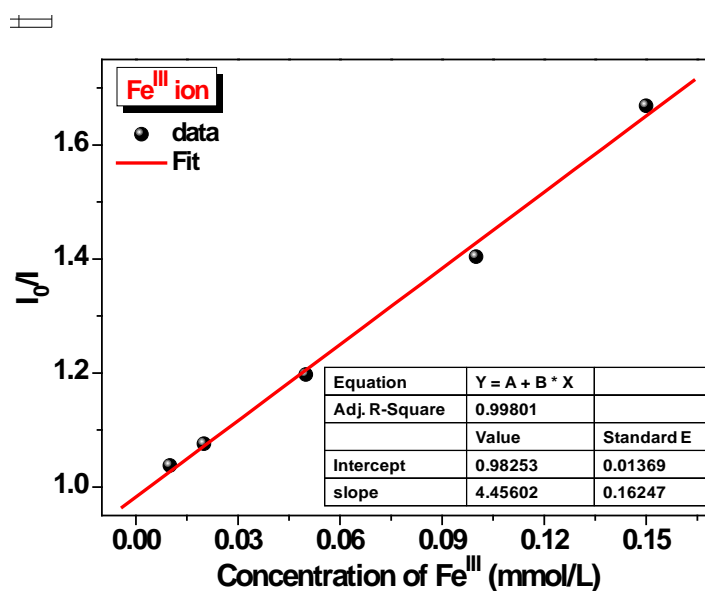
(a)

(b)

Fig. S8 The relationship between the quenching efficiency and the amount of Cr^{III} (a) or Fe^{III} (b) ions.
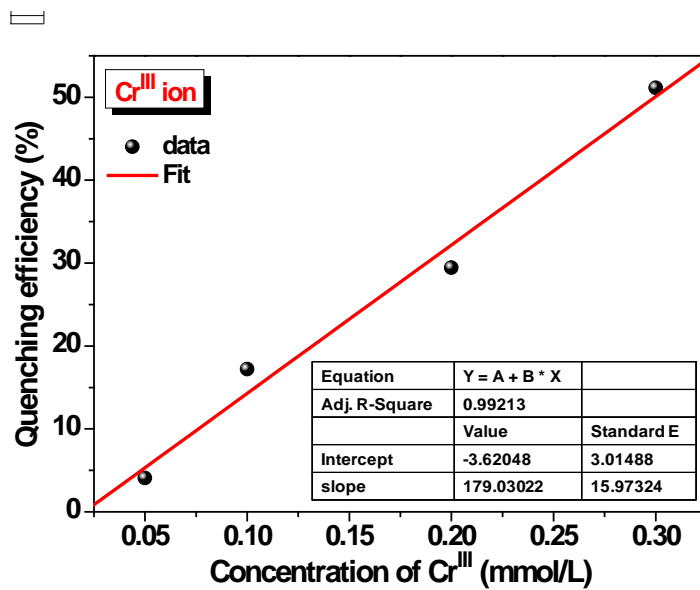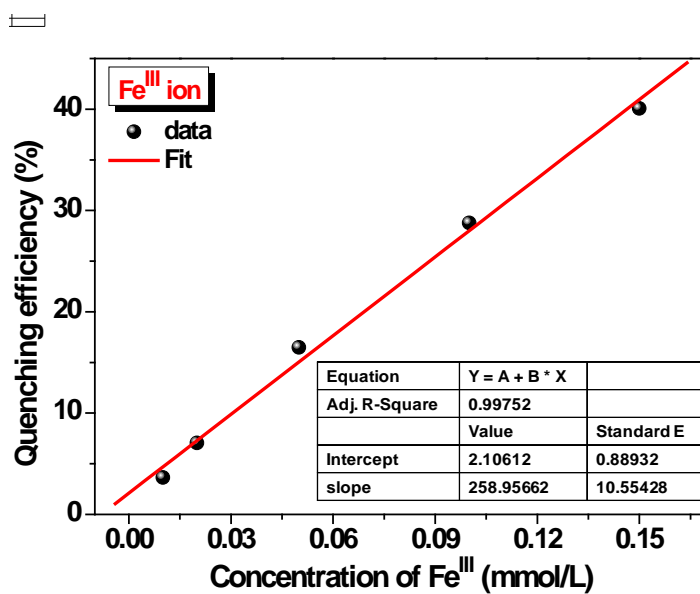
(a)

(b)

Fig. S9 Stern-Volmer (SV) plot for Cr^{III} (a) or Fe^{III} (b) ions in the low concentration range, the red line corresponds to a fit to the linear relationship.

Equation	Y = A + B * X	
Adj. R-Square	0.99213	
	Value	Standard E
Intercept	-3.62048	3.01488
slope	179.03022	15.97324

(a)

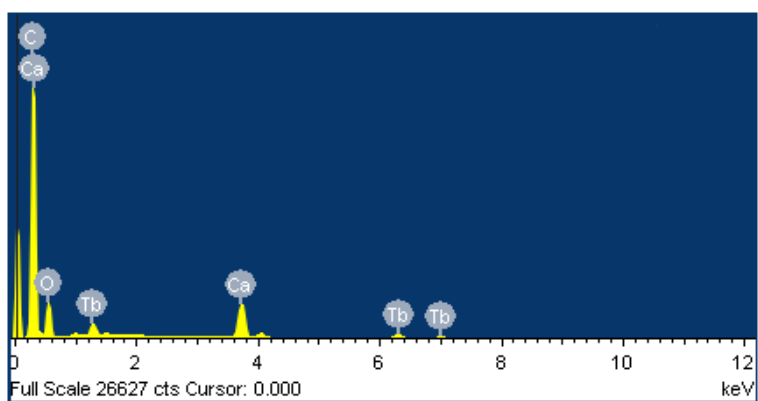| Equation	Y = A + B * X	
Adj. R-Square	0.99752	
	Value	Standard E
Intercept	2.10612	0.88932
slope	258.95662	10.55428

(b)

Fig. S10 Dependence of the quenching efficiency on the concentration of Cr^{III} (a) or Fe^{III} (b) ions in the low concentration range, the red line corresponds to a fit to the linear relationship.
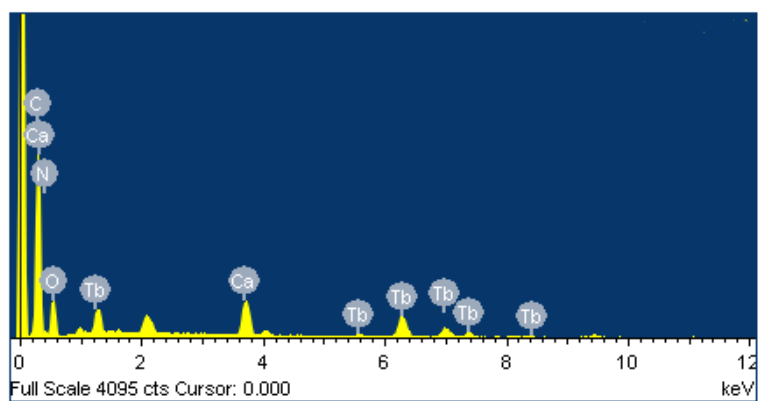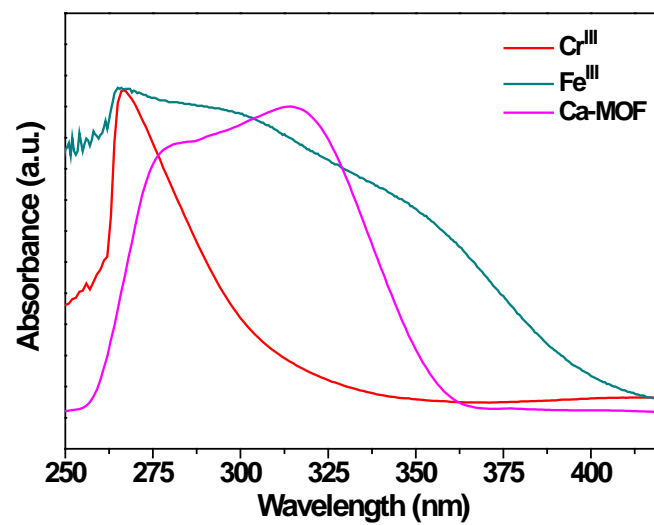
(a)
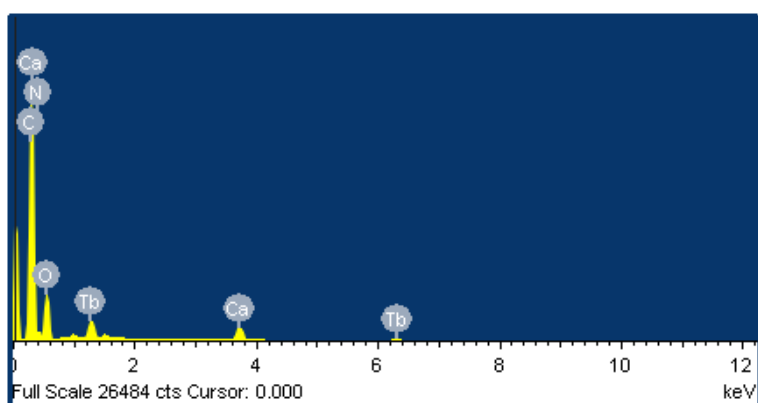
(b)

(c)

Fig. S11 EDS analysis of Tb^{III}@Ca-MOF (a), Tb^{III}@Ca-MOF in Cr^{III} solution (b), and Tb^{III}@Ca-MOF in Fe^{III} solution (c).

Fig. S12 UV–Vis spectra of Cr^{III} and Fe^{III} in DMF and the excitation spectrum of Tb^{III}@Ca-MOF.